Published May 2, 2011

Isolation and function of mouse tissue resident vascular precursors marked by myelin protein zero

Yoshiaki Kubota,[1,2,4] Keiyo Takubo,[1] Masanori Hirashima,[5] Narihito Nagoshi,[3] Kazuo Kishi,[4] Yuji Okuno,[1] Ayako Nakamura-Ishizu,[1] Keigo Sano,[5] Masato Murakami,[6] Masatsugu Ema,[7] Yoshiki Omatsu,[8] Satoru Takahashi,[7] Takashi Nagasawa,[8] Masabumi Shibuya,[6] Hideyuki Okano,[3] and Toshio Suda[1]

[1]Department of Cell Differentiation, The Sakaguchi Laboratory, [2]Center for Integrated Medical Research, [3]Department of Physiology, [4]Department of Plastic Surgery, School of Medicine, Keio University, Shinjuku-ku, Tokyo 160-8582, Japan
[5]Division of Vascular Biology, Department of Physiology and Cell Biology, Kobe University Graduate School of Medicine, Chuo-ku, Kobe, Hyogo 650-0017, Japan
[6]Department of Molecular Oncology, Graduate School of Medicine and Dentistry, Tokyo Medical and Dental University, Bunkyo-ku, Tokyo, 113-8519, Japan
[7]Department of Anatomy and Embryology, Institute of Basic Medical Sciences, Graduate School of Comprehensive Human Sciences, University of Tsukuba, Tsukuba 305-8575, Japan
[8]Department of Immunobiology and Hematology, Institute for Frontier Medical Sciences, Kyoto University, Kyoto 606-8507, Japan

Vasculogenesis describes the process of de novo vessel formation from vascular precursor cells. Although formation of the first major vessels, such as the dorsal aorta and cardinal veins, occurs during embryonic vasculogenesis, the contribution of precursor cell populations to postnatal vessel development is not well understood. Here, we identified a novel population of postnatal vascular precursor cells in mice. These cells express the Schwann cell protein myelin protein zero (Po) and exhibit a $CD45^-CD31^-VEcad^-c\text{-}kit^+CXCR4^+$ surface phenotype. Po^+ vascular precursors (PVPs) are recruited into the growing vasculature, and comprise a minor population of arterial endothelial cells in adult mice. Recruitment of PVPs into growing vessels is mediated by CXCL12–CXCR4 signaling, and is enhanced during vascular expansion induced by Notch inhibition. Po-specific ablation of Flk1, a receptor for VEGF, results in branching defects and insufficient arterial patterning in the retina, as well as reduced neovascularization of tumors and ischemic tissues. Thus, in postnatal mice, although growing vessels are formed primarily by angiogenesis from preexisting vessels, a minor population of arterial endothelia may be derived from tissue-resident vascular precursor cells.

CORRESPONDENCE
Yoshiaki Kubota:
ykubo33@a3.keio.jp
OR
Toshio Suda:
sudato@sc.itc.keio.ac.jp

Abbreviations used: ASMA, arterial smooth muscle actin; EPC, endothelial progenitor cell; IHC, immunohistochemistry; ISH, in situ hybridization; Po, myelin protein zero; PVP, Po^+ vascular precursor; vSMC, vascular smooth muscle cell.

The three processes necessary to form a complete vascular network are vasculogenesis, angiogenesis, and vascular remodeling (Carmeliet, 2003). Generally, vasculogenesis describes the de novo formation of vessels from vascular endothelial precursor cells, which migrate to the location of future vessels, coalesce into cords, and differentiate into lumen-forming endothelial cells. Formation of the first major vessels, such as the dorsal aorta or the cardinal veins, is well known to occur through embryonic vasculogenesis (Risau, 1997). Bone marrow–derived endothelial progenitor cells (EPCs; Asahara et al., 1997) are generally considered to participate in certain aggressive cancer models (Gao et al., 2008), but not in other cancer models or in physiological development (Purhonen et al., 2008). Therefore, increasing attention has been directed to vasculogenesis directed by other lineage cells.

Myelin protein zero (Po) was originally identified as a Schwann cell–specific protein (Lemke and Axel, 1985). Recent studies showed that Po-Cre is expressed by neural crest cells during early embryogenesis (Yamauchi et al., 1999).

Published May 2, 2011

However, different from other neural crest–specific Cre lines (e.g., Wnt1-Cre), Po-Cre marks not only neural crest cells but also some nonneural crest cells (e.g., a minor population of arterial endothelial cells in adult bone marrow); however, it does not mark any endothelial cells during embryogenesis (Nagoshi et al., 2008). This observation suggests that Po expression represents some unknown origin of endothelial cells in postnatal tissues.

Recent studies have demonstrated that some neural or mesenchymal lineage cells resident in certain tissues have a potential to differentiate into endothelial cells in in vitro and in vivo, suggesting the existence of tissue-resident vascular precursor cells (Beltrami et al., 2003; Planat-Benard et al., 2004; Wurmser et al., 2004; Grenier et al., 2007). In human fetal retinas, morphological analysis has suggested that tissue-resident retinal "angioblasts" participate in the growth of retinal vessels. The retinal angioblasts are characterized by an expression profile of $CD39^+CXCR4^+ckit^+$ or $CD45^-CD31^-$ and a positivity for Nissl staining (Henking and De Oliveira, 1967; Ashton, 1970; McLeod et al., 2006). However, these studies have investigated neither angioblast endothelial potential nor their actual contribution toward retinal vessels. Moreover, retinal angioblasts lack in situ expression of Flk-1, the earliest marker for endothelial cell precursors (Millauer et al., 1993; Fruttiger, 2002). Therefore, retinal vascularization is currently considered to consist of angiogenic growth lacking the participation of precursor cell populations (Gariano and Gardner 2005).

The ability to effectively track cell fates throughout development depends on the fidelity and permanence of the labeling system used. Cell fate mapping of nonmammalian cells has been performed using quail-chick chimeras or vital dye labeling (Stern and Fraser, 2001; Etchevers et al., 2001). However, these systems are not effective for determining the long-term fates of cells in mammals. The use of Cre-loxP–based techniques has recently provided the necessary breakthrough for mapping progenitor–progeny cell relationships in mice (Stern and Fraser, 2001).

In this paper, we used Cre-loxP–based cell fate mapping to show that Po^+ tissue-resident vascular precursors are recruited into the growing vasculature and comprise a minor population of the arterial endothelial cells in adults. We also show that Po^+ vascular precursors (PVPs) are substantially vital not only for retinal vascularization but also for neovascular formation in ischemic tissues and tumor angiogenesis.

RESULTS

Po-Cre marks endothelial cells and spindle-shaped cells in avascular areas

The initial step in our study was to examine the distribution of GFP^+ cells in *Po-Cre*$^+$*Flox-CAT-EGFP* mice undergoing postnatal retinal angiogenesis. In a preliminary study, we did not detect any abnormality in *Po-Cre*$^+$*Flox-CAT-EGFP* mice (unpublished data). GFP was detected in endothelial cells, desmin$^+$ pericytes/vascular smooth muscle cells (vSMCs) and spindle-shaped cells in avascular areas (Fig. 1, A–J). Moreover, some spindle-shaped GFP^+ cells were directly associated with endothelial tip cell filopodia (Fig. 1, E–G). Unlike pericytes, GFP^+ spindle-shaped cells were negative for NG2 and PDGFRβ and were localized abluminally to the vascular basal lamina (Fig. S1 A). GFP^+ endothelial cells were restricted to arteries with a ladderlike pattern in adulthood and were detected in endothelial lumens (Fig. 1, K–P). FACS analysis indicated that $4.88 \pm 1.84\%$ ($n = 5$) of all $CD31^+$ cells were GFP^+ in adult (Fig. 1 Q), and most GFP^+CD31^+ cells were VE-cadherin$^+$Tie-2$^+$ endothelial cells (unpublished data). Outside the retina, GFP was also detected in endothelial cells, pericytes/vSMCs, and spindle-shaped cells (Fig. 1, R–T). To check whether these GFP^+ cells in *Po-Cre*$^+$*Flox-CAT-EGFP* mice are neural crest-derived or not, we examined two lines of transgenic mice, *Wnt1-Cre,* and human tissue plasminogen activator (*Ht-PA)-Cre*. We found that pericytes, but not spindle-shaped cells and endothelial cells, were marked by these two Cre lines (Fig. 1, U–X). A previous cell fate–mapping study using quail/chick chimeras (Etchevers et al., 2001) agrees with our finding that neural crest cells give rise to pericytes, but not to endothelial cells. Collectively, Po-Cre, but not *Wnt1-Cre* and *Ht-PA-Cre,* marked endothelial cells and spindle-shaped cells in avascular areas.

Spindle-shaped angioblasts express Po and differentiate into endothelial cells in vivo and in vitro

We further characterized GFP^+ spindle-shaped cells in *Po-Cre*$^+$*Flox-CAT-EGFP* mice. At first, we expected these GFP^+ spindle-shaped cells in the avascular area are some neural or hematopoietic lineage cells. However, multiple marker analyses showed that these cells were not astrocytes, ganglion cells, photoreceptors, or monocyte/macrophages (Fig. S1, B and C). Instead, these spindle cells possessed the features of classically termed retinal "angioblasts." They were positive for CD39 and Nissl, and slowly divided compared with surrounding cells such as astrocytes and ganglion cells (Fig. 2, A and B). The results that nonneural crest cells marked by Po involve angioblasts and a certain percentage of endothelial cells suggested that these cells express Po and have the potential to drive Cre-recombinase in *Po-Cre* mice. In situ hybridization (ISH) showed that Po transcripts (Fig. 2, C and D) were abundantly detected in spindle-shaped angioblasts in avascular areas, but not in any endothelial cells or pericytes. As shown in Fig. 1 (A–J), retinas of *Po-Cre*$^+$*Flox-CAT-EGFP* mice showed GFP expression in endothelial cells, pericytes, and retinal angioblasts. Thus, we isolated $GFP^+CD31^-PDGFR\beta^-$ cells from *Po-Cre*$^+$*Flox-CAT-EGFP* mice by FACS and treated this population as angioblasts. Quantitative PCR analysis of FACS-sorted cells showed that *mpz*, the gene that encodes Po, was expressed in $GFP^+CD31^-PDGFR\beta^-$ cells, but far less in GFP^+ or $CD31^+PDGFR\beta^-$ cells (Fig. 2 E). As there remains a possibility that postnatal GFP^+ endothelial cells could originate from Po-expressing embryonic endothelial cells, we examined embryonic Po-Cre expression. The possibility was negated by the fact that numerous GFP^+ cells were only detected

Published May 2, 2011

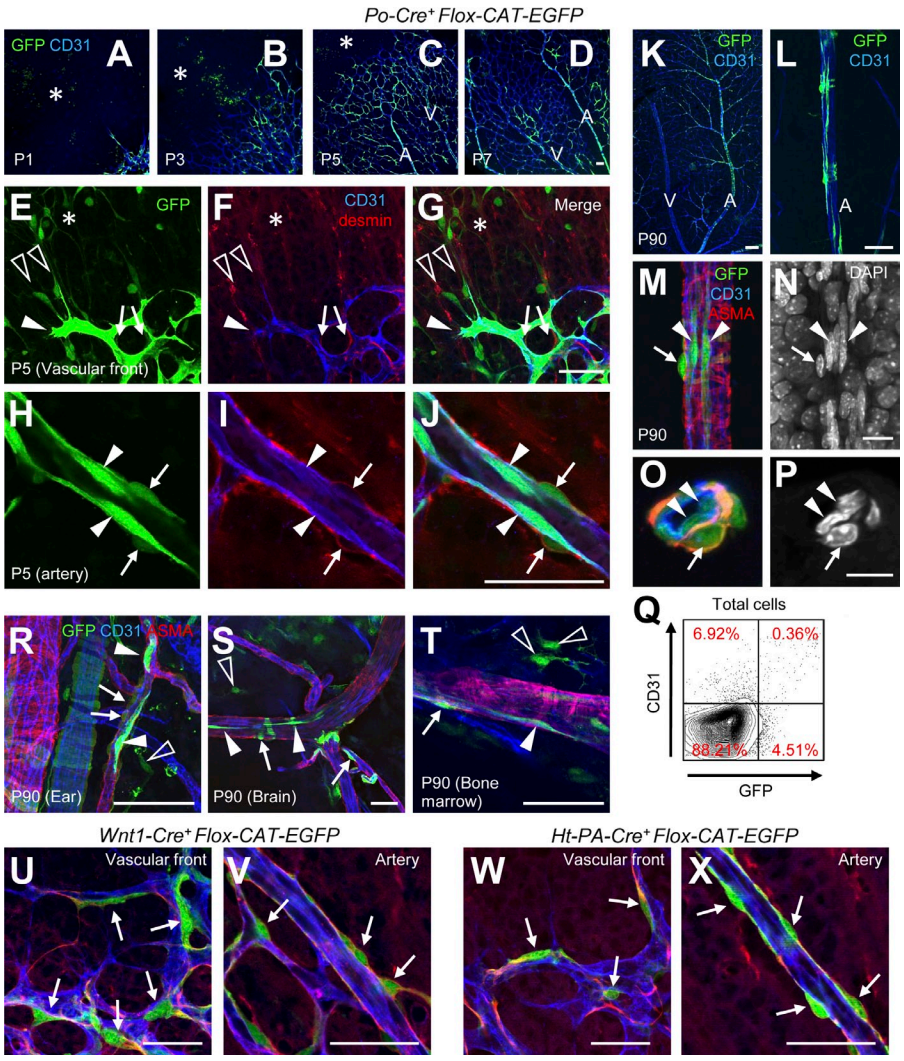

Figure 1. Po-Cre marks endothelial cells and spindle-shaped cells in avascular areas. (A–L) Triple IHC for GFP (green), CD31 (blue), and desmin (red) in retinas of *Po-Cre*$^+$*Flox-CAT-EGFP* mice at postnatal day (P) 1, 3, 5, 7, and 90. Representative images from at least three independent experiments. GFP$^+$ spindle-shaped cells in the avascular area (asterisks), endothelial cells (closed arrowheads), and pericytes/smooth muscle cells (arrows). A, arterial areas; V, venous areas. GFP$^+$ spindle-shaped cells associated with filopodia of endothelial tip cells, open arrowheads in E–G. (M–P) Quadruple IHC for GFP (green), CD31 (blue), ASMA (red), and DAPI (white) in retinas of adult *Po-Cre*$^+$*Flox-CAT-EGFP* mice. O and P are images from a cross section. Representative images from three independent experiments. GFP$^+$ lumen-forming endothelial cells (arrowheads) and smooth muscle cells (arrows). (Q) FACS analysis of dissociated retinal cells from adult *Po-Cre*$^+$*Flox-CAT-EGFP* mice. 4.88 ± 1.84% (n = 5) of CD31$^+$ cells were GFP$^+$. (R–T) Triple IHC for GFP (green), CD31 (blue), and ASMA (red) in various tissues from adult *Po-Cre*$^+$*Flox-CAT-EGFP* mice. GFP$^+$ endothelial cells (closed arrowheads), pericytes/vSMCs (arrows), and spindle-shaped cells in the avascular area (open arrowheads). Representative images from three independent experiments. (U–X) Triple IHC for GFP (green), CD31 (blue), and desmin (red) at P4 in *Wnt1-Cre/Flox-CAT-EGFP* mice (U and V) or *Ht-PA-Cre/Flox-CAT-EGFP* mice (W and X). Representative images from seven independent experiments. GFP$^+$ pericytes/smooth muscle cells are indicated by arrows. Bars: (A–D, K, and L) 100 µm; (E–J and R–X) 50 µm; (M–P) 10 µm.

in Sox10$^+$ or p75$^+$ neural crest cells, but not in endothelial cells (Fig. S2, A–K), and that GFP$^+$ cells were not detected in any pericytes or vSMCs (Fig. S2, L–O). FACS-sorted GFP$^+$ angioblasts are negative for CD45 and VE-cadherin, but are positive for c-kit, CXCR4, Flk-1, and FGFR1 (Fig. 2 F), which are markers for embryonic hemangioblasts or endothelial progenitors (Millauer et al., 1993; Guo et al., 2006). In comparison to reported multipotent stem cells, such as very small embryonic-like stem cells (Ratajczak et al., 2008) and multipotent adult progenitor cells (Jiang et al., 2002), GFP$^+$ angioblasts express CD133 but not SSEA-1 (Fig. 2 F). Collectively, the Cre-loxP–based fate-mapping study suggested that angioblasts express Po-mRNA and give rise to endothelial cells. So far, the concept of angioblasts has lacked the evidence that they actually differentiate into endothelial cells. Therefore, we cultured FACS-sorted GFP$^+$ angioblasts in endothelial culture conditions. After 4 d, they gave rise to CD31$^+$ cells (Fig. 2 G) that expressed endothelial cell markers such as VE-cadherin, Flk-1, and EphrinB2, but not CD45 (Fig. 2, H–K). Next, we performed intraocular transplantation of FACS-sorted angioblasts into wild-type mice, and tracked their cell fate. 5 d after transplantation, they differentiated into endothelial cells, but not pericytes (Fig. 2 L). In FACS analysis, GFP$^+$CD31$^+$ cells, but not GFP$^+$PDGFRβ$^+$ cells, were detected in the recipient retinas (Fig. 2, M and N). Considering the capacities for endothelial differentiation in vitro and in vivo, we designated these GFP$^+$ angioblasts as PVPs. Perivascular spindle-shaped cells marked by Po-Cre, similar to PVPs in the retina, existed in nonretinal tissues (Fig. 1, R–T). We suspected that these cells possess the characteristics of vascular precursor cells. GFP$^+$CD31$^-$PDGFRβ$^-$ isolated from subcutaneous tissues of adult *Po-Cre*$^+$*Flox-CAT-EGFP* mice were incorporated into the growing vessels in transplanted tumors (S-180) and ischemic flaps (Fig. 2, O–Q). This data suggests that PVPs were present in subcutaneous tissues.

Recruitment of PVPs is mediated by CXCR4 signaling

A previous finding regarding the bone marrow–derived CXCR4$^+$ hemangiocytes (Jin et al., 2006) prompted us to study the involvement of CXCL12–CXCR4 signaling in the

Published May 2, 2011

recruitment of PVPs. We examined the expression pattern of CXCL12 in the developing retina using *CXCL12*$^{+/EGFP}$ knock-in mice. Surprisingly, CXCL12 was predominantly expressed in vascularized areas rather than avascular areas (Fig. 3, A–C). The major CXCL12-expressing cells were astrocytes, and CXCL12 was not expressed by microglia or

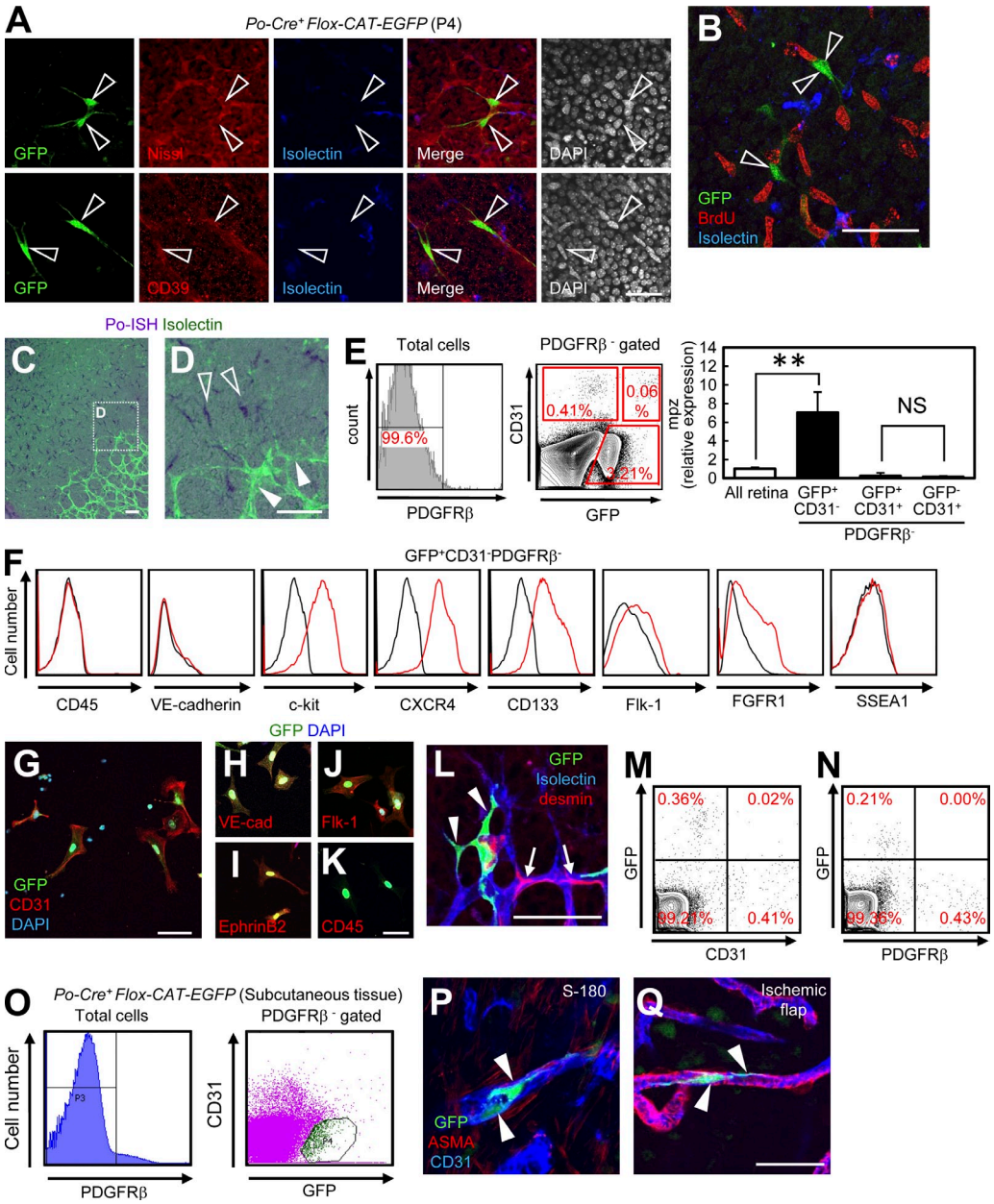

Figure 2. Spindle-shaped angioblasts express Po and differentiate into endothelial cells in vivo and in vitro. (A and B) IHC of retinas from *Po-Cre*$^{+}$*Flox-CAT-EGFP* mice at P4 stained with indicated antibodies. Representative images from three independent experiments. GFP^{+} spindle-shaped cells (open arrowheads). (C and D) ISH for Po (purple) combined with isolectin staining (green) at P3. Representative images from three independent experiments. Spindle-shaped cells in the avascular area (open arrowheads). Endothelial cells (closed arrowheads). (E) Quantitative PCR analysis of *mpz* expression in FACS-sorted retinal cells at P3 ($n = 6$). (F) FACS analysis of dissociated retinal cells from *Po-Cre*$^{+}$*Flox-CAT-EGFP* mice at P3. Representative plots from at least three independent experiments. Black histograms, isotype control staining. (G–K) GFP^{+}CD31^{-}PDGFRβ^{-} cells from *Po-Cre*$^{+}$*Flox-CAT-EGFP* mice at P3 stained with indicated antibodies after 4 d of culture. Representative images from at least three independent experiments. (L) FACS-sorted GFP^{+}CD31^{-}PDGFRβ^{-} cells from P3 *Po-Cre*$^{+}$*Flox-CAT-EGFP* mice were intraocularly transplanted into recipient mice at P1, and sacrificed at P6. GFP^{+} endothelial cells, closed arrowheads; pericytes, arrows. Representative images from 10 independent experiments. (M and N) FACS analysis of dissociated retinal cells from mice intraocularly transplanted with FACS-sorted GFP^{+}CD31^{-}PDGFRβ^{-} cells at P1. Representative plots from three independent experiments. (O) FACS plots of dissociated cells from subcutaneous tissues of adult *Po-Cre*$^{+}$*Flox-CAT-EGFP* mice. Representative plots from three independent experiments. (P and Q) GFP^{+}CD31^{-}PDGFRβ^{-} cells were transplanted into the S-180 tumors and ischemic flaps. Representative images from three independent experiments. GFP^{+} endothelial cells, closed arrowheads. Bars, 50 µm. **, $P < 0.01$.

Published May 2, 2011

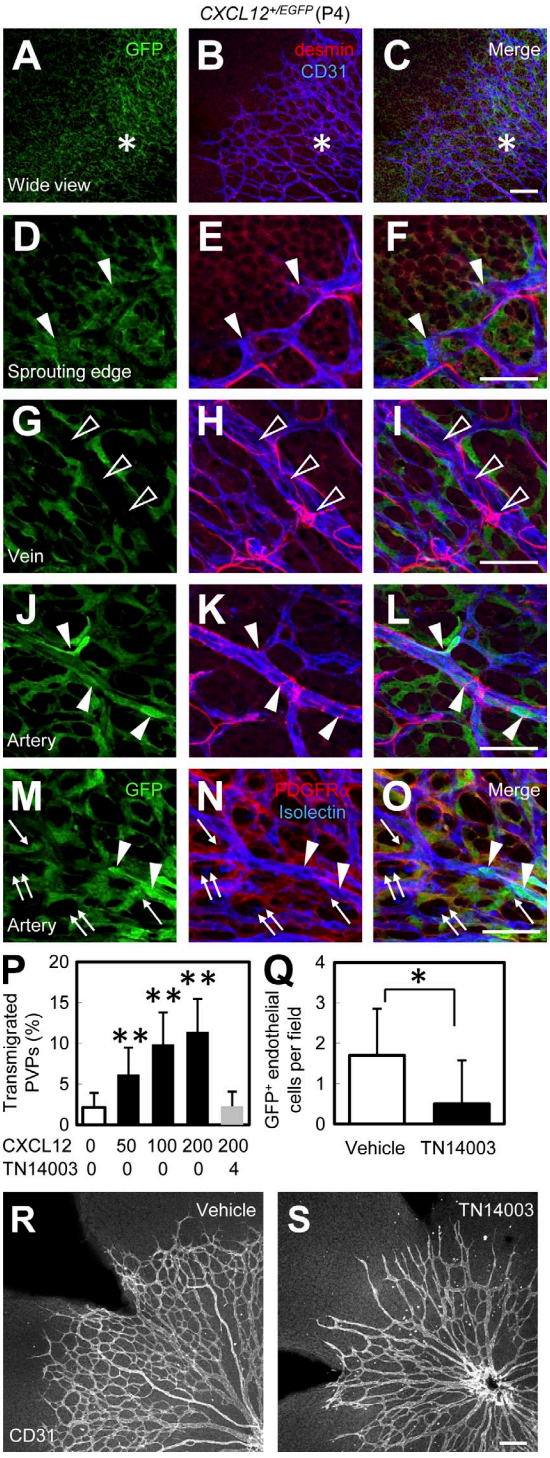

Figure 3. Recruitment of PVPs is mediated by CXCR4 signaling. (A–O) IHC in the retina of *CXCL12*$^{+/EGFP}$ mice at P4. Representative images from three independent experiments. Vascularized area is represented by asterisks. Tip cells are indicated by arrowheads in D–F. Arterial endothelial cells are indicated by arrowheads in J–L. Astrocytes are indicated by arrows. Venous endothelial cells are indicated by open arrowheads in G–I. Microglia are indicated by double arrows. (P) In vitro chemotaxis assay of isolated PVPs (GFP$^+$CD31$^-$PDGFRβ$^-$; $n = 4$). CXCL12 was added at indicated doses to the lower chamber. Preincubation with TN14003 (CXCR4-specific antagonist) were performed when indicated. (Q) Quantification of GFP$^+$ endothelial cells per field ($n = 10$) in recipient retinas (P5) intraocularly transplanted with Vehicle or TN14003-treated GFP$^+$CD31$^-$PDGFRβ$^-$ cells at P3. (R and S) Retinas from *Po-Cre*$^+$*Flox-CAT-EGFP* mice (P4) continuously treated with vehicle or TN14003 (P1-4) were stained with anti-CD31. Representative images from three independent experiments. Bars, 100 µm. *, $P < 0.05$; **, $P < 0.01$.

pericytes (Fig. 3, M–O). Moreover, CXCL12 expression was detected in arterial endothelial cells and tip cells, but not venous endothelial cells (Fig. 3, D–L). In in vitro chemotaxis assay, CXCL12 increased chemotaxis of FACS-sorted PVPs in a dose-dependent manner, and the chemotactic effect was abrogated by pretreatment of cells with CXCR4-specific antagonist (TN14003; Fig. 3 P). Pretreatment of isolated PVPs with TN14003 significantly decreases incorporation of transplanted PVPs into recipient vasculature (Fig. 3 Q). Systemic treatment of mice with TN14003 led to formation of a sparse vascular network (Fig. 3, R and S). Yet it is unclear whether this vasoinhibitory effect was owed to PVPs or mature endothelial cells. These results suggest that the recruitment of PVPs is mediated through CXCR4 signaling.

Recruitment of PVPs is enhanced during vascular expansion induced by Notch inhibition

Dll4-Notch1 signaling is known to regulate vascular patterning by inducing endothelial tip cell conversion into stalk cells (Hellström et al., 2007; Suchting et al., 2007). We used a γ-secretase inhibitor, DAPT, which is widely used for analyzing vascular changes induced by Notch inhibition (Hellström et al., 2007; Tammela et al., 2008). When *Po-Cre*$^+$*Flox-CAT-EGFP* mice were treated with DAPT, GFP$^+$ endothelial tip cells were increased and GFP$^+$ stalk cells were decreased at 3–6 h after administration (Fig. 4, A and B). The GFP$^+$ tip/stalk ratio peaked at 3–6 h after DAPT injection. At 12–48 h after administration, both GFP$^+$ stalk cells and tip cells had increased (Fig. 4, C-F). DAPT significantly increased not only the number of GFP$^+$ endothelial cells but also their Flk-1 expression (Fig. 4 H). Endothelial CXCL12 expression is upregulated 12 h after DAPT administration (Fig. 4 I), which may account for a delayed increase in the recruitment of PVPs into the vasculature. When mice were subjected to continuous DAPT treatment, GFP$^+$ endothelial cells were dramatically increased in number, but remained in the capillary plexus, and their incorporation into arteries was inhibited (Fig. 4, J, K, and N). Inhibition of Dll4/Notch signaling by the application of Dll4-neutralizing antibodies increased GFP$^+$ endothelial cells (Fig. S3, A–C) in a manner similar to DAPT treatment. First, we suspected that anti-Dll4 antibodies directly affect the behavior of PVPs. However, Dll4 and Notch1 were expressed only in mature endothelial cells, and not in PVPs (Fig. 4 P). Moreover, anti-Dll4 antibodies did bind to endothelial cells, but not to PVPs (Fig. S3, D–I), suggesting that Dll4 inhibition does not affect PVPs directly. To assess the effect of enhanced Notch signaling, we used a Jag1 peptide, which is

Published May 2, 2011

widely used for analyzing vascular changes induced by Notch gain-of-function (Hellström et al., 2007). Continuous administration of a Jag1 peptide significantly decreased the number of GFP$^+$ endothelial cells (Fig. 4, L, M, and O). Collectively, recruitment of PVPs was enhanced during vascular expansion induced by Notch inhibition. However, the effect of Notch inhibition on PVPs is likely to be an indirect one, and partly mediated by the up-regulation of CXCL12 in endothelial cells.

Po-conditional Flk-1 knockout mice show defective vascular branching and arterial patterning

VEGF/Flk-1 signaling is essential for endothelial survival/proliferation, tip cell formation, and arterial patterning (Shalaby et al., 1995; Lawson et al., 2002; Gerhardt et al., 2003; Jakobsson et al., 2010). To characterize the physiological roles of PVP-derived endothelial cells during vascular patterning, we generated mice with a Po-specific conditional knockout of Flk1

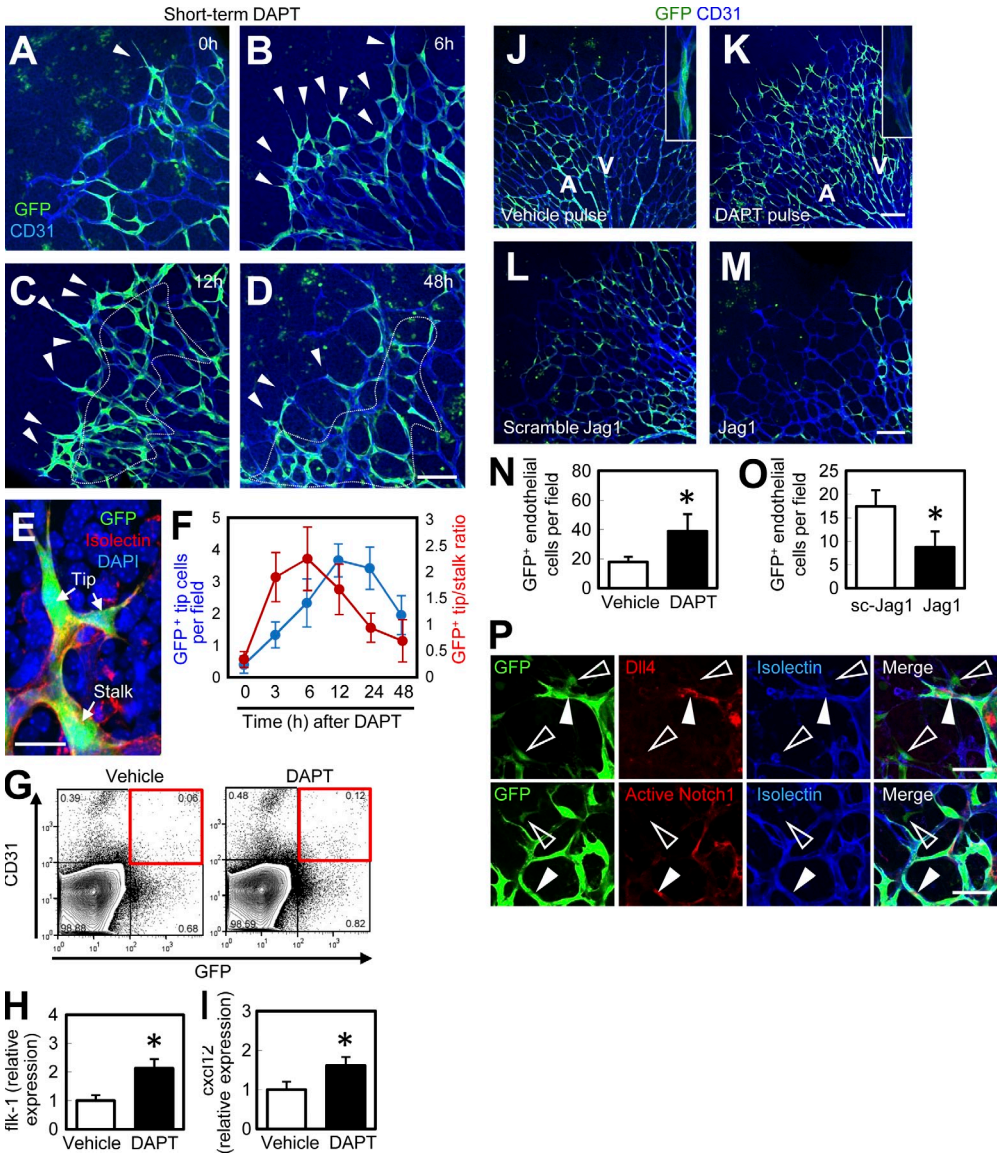

Figure 4. Recruitment of PVPs is enhanced during vascular expansion induced by Notch inhibition. (A–D) IHC for GFP (green) and CD31 (blue) after subcutaneous injection of DAPT at P4. GFP$^+$ tip cells are indicated by arrowheads. Stalk cells are indicated by the area within the dashed line. Representative images from six independent experiments. (E) An image for discriminating GFP$^+$ tip cells and stalk cells. (F) Quantification of GFP$^+$ tip cells or GFP$^+$ tip/stalk cell ratios ($n = 6$). (G and H) Quantitative *flk-1* expression analysis in FACS-sorted GFP$^+$CD31$^+$ cells gated on PDGFRβ$^-$ cells in the retinas of *Po-Cre$^+$Flox-CAT-EGFP* mice at P4 12 h after vehicle or DAPT administration ($n = 7$). (I) Quantitative PCR analysis of *cxcl12* in FACS-sorted CD31$^+$ cells 12 h after vehicle or DAPT treatment ($n = 7$). (J and K) P4 retinas of *Po-Cre$^+$Flox-CAT-EGFP* mice after continuous vehicle or DAPT treatment (P1–4). Insets indicate arterial areas. Representative images from eight independent experiments. (L and M) P5 retinas of *Po-Cre$^+$Flox-CAT-EGFP* mice after pulse treatment from P1 to P5 with scramble Jag1 peptides (L) or Jag1 peptides (M). Representative images from eight independent experiments. (N and O) Quantification of GFP$^+$ endothelial cells ($n = 8$). (P) IHC of retinas from *Po-Cre$^+$Flox-CAT-EGFP* mice at P4 stained with indicated antibodies. Representative images from three independent experiments. Closed arrowheads, mature endothelial cells; open arrowheads, PVPs. Bars: (A–D, J–M, and P) 100 µm; (E) 20 µm. *, $P < 0.05$.

Published May 2, 2011

(*Po-Cre/Flox-flk1*: termed "*Flk-1*$^{Po\text{-}CKO}$ mice"). In a preliminary study, *Po-Cre*$^{-}$*Flk-1*$^{Flox/lacZ}$ mice did not show significant defects compared with *Po-Cre*$^{-}$*Flk-1*$^{Flox/+}$ or *Po-Cre*$^{+}$*Flk-1*$^{Flox/+}$ littermates (unpublished data). The retinas of *Flk-1*$^{Po\text{-}CKO}$ mice at P4 showed significantly decreased vascular branching, although the decrease in tip cell number was only moderate (Fig. 5, A, B, and K–M). Arterial patterning was incomplete and blood flow was poor in the retinas of *Flk-1*$^{Po\text{-}CKO}$ mice (Fig. 5, C, D, and N). Although recruitment of desmin^{+} pericytes was normal, expression of arterial smooth muscle actin (ASMA) was reduced in *Flk-1*$^{Po\text{-}CKO}$ mice (Fig. 5, E–H, and O). The observation of increased numbers of PVP-derived capillary endothelial cells after Notch inhibition (Fig. 4, J and K) prompted us to examine vascular abnormalities of *Flk-1*$^{Po\text{-}CKO}$ mice after DAPT treatment. When *Flk-1*$^{Po\text{-}CKO}$ mice were continuously administered DAPT, they exhibited severe irregularities in vasculature patterning (Fig. 5, I and J). In agreement with a previous work (Jakobsson et al., 2010), Flk-1 expression, determined by GFP expression in *Flk-1*$^{+/EGFP}$ knock-in mice (Ema et al., 2006), was expressed in endothelial cells, Muller cells, and photoreceptors in the outer nuclear layer, but not in spindle-shaped angioblasts (Fig. S4, A and C). The Flk-1 expression in *Flk-1*$^{Po\text{-}CKO}$ mice showed reduction in endothelial cells but not in Muller cells (Fig. S4, B and D). To rule out the effects of Flk-1 inactivation in other cells, such as neural crest cells, we thoroughly examined Flk-1 expression. We could not detect Flk-1 expression in neural crest cells, neurons, Schwann cells, vSMCs, or pericytes throughout the body except for in the central nervous system (Fig. S5). However, as even undetectable levels of Flk-1 expression in neural crest cells may be vital, we generated Wnt1-specific Flk-1 knockout (*Flk-1*$^{Wnt1\text{-}CKO}$) mice (*Wnt1-Cre*$^{+}$*Flk-1*$^{Flox/Flox}$). Wnt1-Cre is expressed in neural crest cells (Danielian et al., 1998; Nagoshi et al., 2008) and all pericytes/vSMCs in the retinas of mice at P4. *Flk-1*$^{Wnt1\text{-}CKO}$ mice develop normally and do not exhibit any vascular defects in their postnatal retina (Fig. 5, P–U). Therefore, vascular defects in *Flk-1*$^{Po\text{-}CKO}$ mice are likely caused by impairment in PVPs and PVP-derived endothelial cells rather than defects in neural crest cells or pericytes/vSMCs. *Flk-1*$^{Po\text{-}CKO}$ mice showed significantly decreased endothelial proliferation, increased endothelial apoptosis, and increased empty basement membrane sleeves that are positive for collagen IV, but lacking endothelial markers, such as isolectinB4, which consistently highlight vessel regression (Phng et al., 2009; Fig. S6).

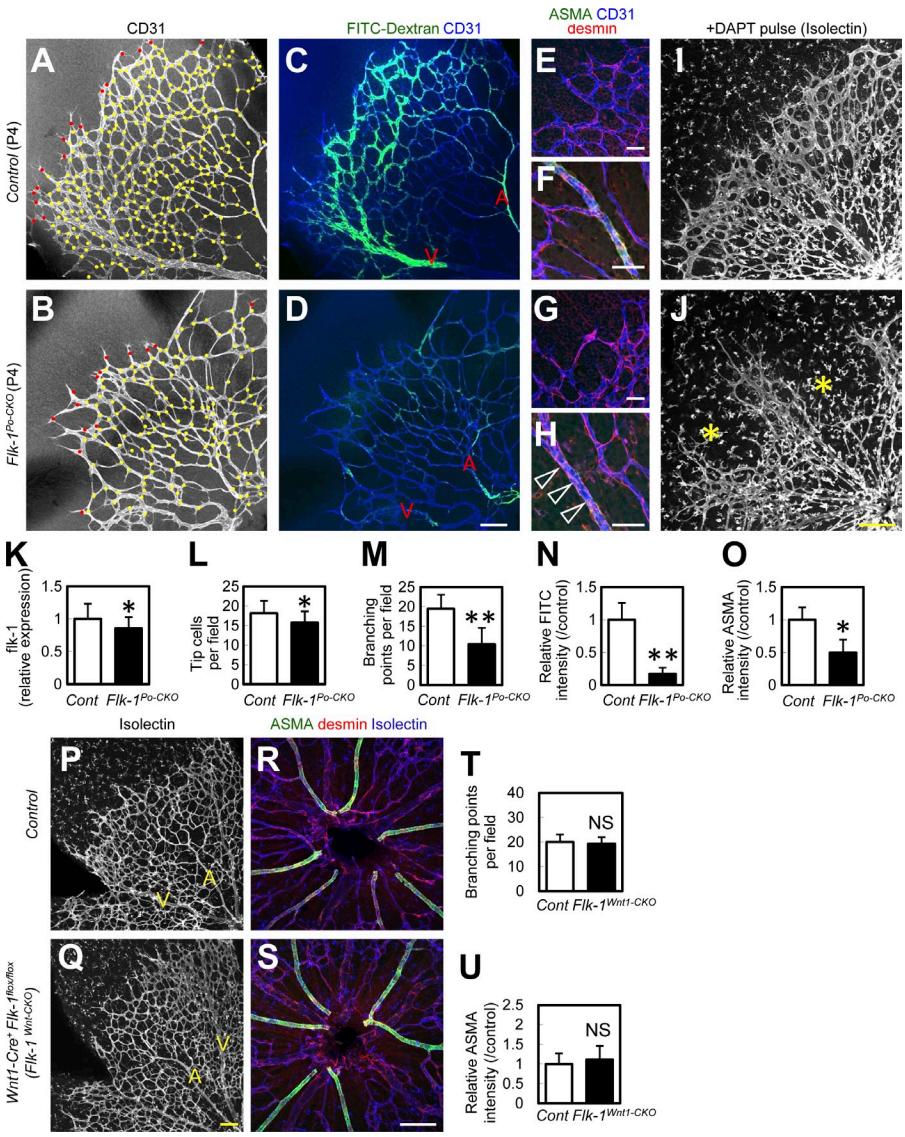

Figure 5. Po-conditional Flk-1 knockout mice show branching defects and insufficient arterial patterning. (A–D) Perfusion staining of blood flow (green) combined with CD31 staining (white in A and B; blue in C and D). Representative images from eight independent experiments. Red dots, tip cells. Yellow dots, branching points. Arteries, A. Veins, V. (E–H) Triple IHC for ASMA (green), desmin (red), and CD31 (blue). Smooth muscle cells (open arrowheads in H). Representative images from eight independent experiments. (I and J) P4 retinas after continuous DAPT treatment (P1–4). Asterisks indicate severely obliterated areas. Representative images from three independent experiments. (K–O) Quantification of relative *flk-1* expression ($n = 5$), tip cells ($n = 8$), branching points ($n = 8$), relative FITC intensity ($n = 8$), and relative ASMA intensity ($n = 8$). (P–S) Triple IHC for ASMA (green), Isolectin (white in P and Q; blue in R and S), and desmin (red) at P4. Representative images from six independent experiments. (T and U) Quantification ($n = 6$). Bars: (A–D, I, J, and P–S) 100 µm; (E–H) 50 µm. *, $P < 0.05$; **, $P < 0.01$.

Published May 2, 2011

PVPs contribute to neovascular formation into ischemic tissues and tumor angiogenesis

Reportedly, rapidly expanding vasculature at the capillary level seen during Notch inhibition mimics the pathological state of the vasculature in disease states such as cancer (Noguera-Troise et al., 2006; Ridgway et al., 2006). The increased functional contribution of PVP-derived endothelial cells after Notch inhibition as seen in retinal vessels (Fig. 4 K and Fig. 5, I and J) prompted us to examine their roles in tumor angiogenesis. To examine the role of PVPs in a cancer model, murine tumor cells (S-180) were transplanted subcutaneously into the bilateral axillae of *Po-Cre*$^{+}$*Flox-CAT-EGFP* mice. GFP^{+} endothelial cells were more abundant in the tumor vasculature than in surrounding subcutaneous tissues (Fig. 6, A and B). *Flk-1*$^{Po\text{-}CKO}$ mice transplanted with S-180 cells showed reduced tumor growth and less tumor angiogenesis than control mice transplanted with S-180 cells (Fig. 6, E, F, I, J, and M). To induce ischemic areas in adult tissues outside the retina, we used the ischemic skin flap model. GFP^{+} endothelial cells in *Po-Cre*$^{+}$*Flox-CAT-EGFP* mice were abundant in collateral vessels 7 d after flap elevation (Fig. 6, C and D). Wider necrotic areas and decreased collateral vessel formation was observed in *Flk-1*$^{Po\text{-}CKO}$ mice compared with control mice (Fig. 6, G, H, K, and L). Collectively, PVP-derived endothelial cells contribute to the neovascular formation in ischemic tissues and tumor angiogenesis.

DISCUSSION

In this study, we identified tissue-resident vascular precursors marked by Po. During physiological development, PVPs were recruited into the growing vasculature, and comprised a minor population of the arterial endothelial cells in adults. CXCL12–CXCR4 signaling mediates recruitment of PVPs into the vessels. Tip/stalk transition of PVP-derived endothelial cells is regulated by Dll4/Notch1 signaling.

A previous study clearly showed that retinal angioblasts lack detectable Flk-1 expression in ISH (Fruttiger, 2002). In contrast, our FACS analysis revealed weak Flk-1 expression in PVPs, although we failed to detect Flk-1 expressions using immunohistochemistry. This controversy is likely caused by the difference in the detection method used. FACS analysis may be more sensitive than ISH and immunohistochemistry (IHC) in detecting Flk-1 expression. In this regard, vascular defects in *Flk-1*$^{Po\text{-}CKO}$ mice are likely caused by decreased endothelial proliferation, increased endothelial apoptosis, and excessive vascular regression in stalk cells, rather than defective tip cells (i.e., defective differentiation of PVPs). Considering that vascular regression is highly dependent on the VEGF–Notch–Nrarp pathway

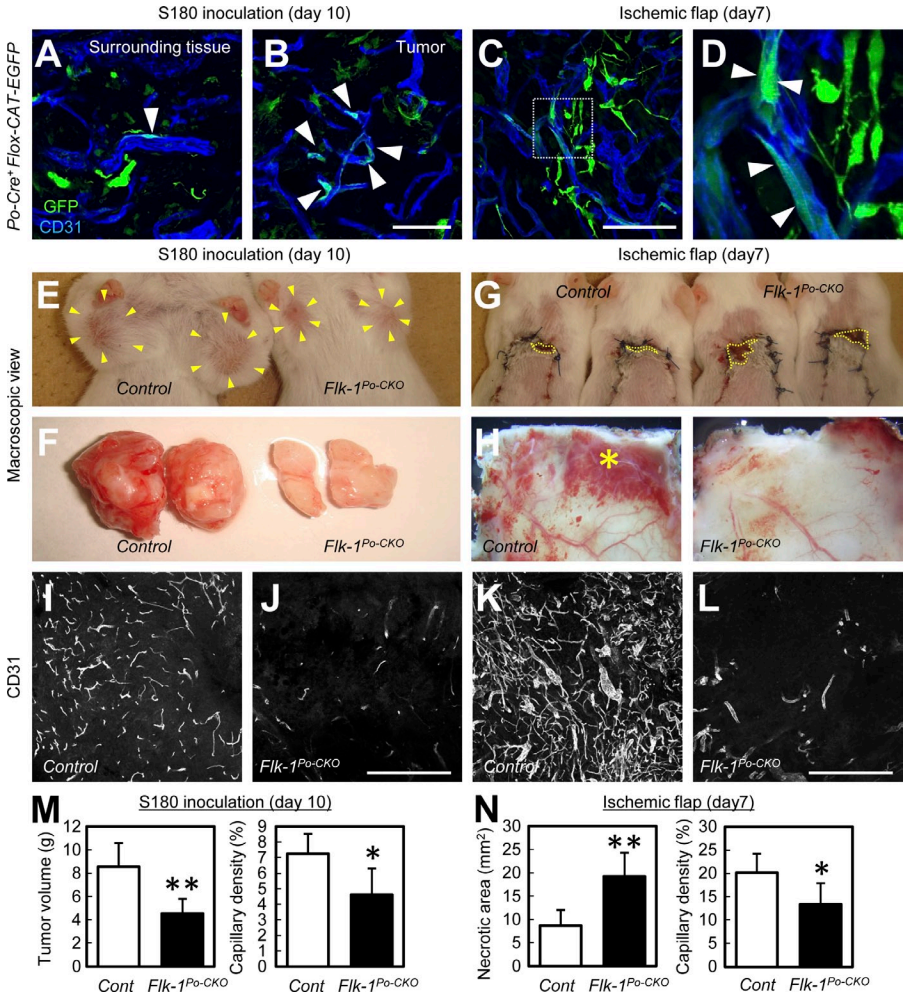

Figure 6. PVPs functionally contribute to tumor angiogenesis and neovascular formation into ischemic flaps. (A–D) Tumors or surrounding tissues 10 d after transplantation of S-180 cells, or ischemic flap tissues 7 d after flap elevation in adult *Po-Cre*$^{+}$*Flox-CAT-EGFP* mice. Arrowheads, GFP^{+} endothelial cells. Representative images from at least three independent experiments. (E–H) Macroscopic view of tumors 10 d after transplantation of S-180 cells, or ischemic flap tissues 7 d after flap elevation in adult control or *Flk-1*$^{Po\text{-}CKO}$ mice. Representative images from 12 independent experiments. Tumors in E are indicated by arrowheads. Necrotic areas in G are indicated by dotted line areas. The asterisk in H indicates collateral vessels. (I–L) Representative sections of tumors 10 d after transplantation of S-180 cells, or ischemic flap tissues 7 d after flap elevation in adult control or *Flk-1*$^{Po\text{-}CKO}$ mice. Representative images from 12 independent experiments. (M and N) Quantification of tumor volume, necrotic area in the ischemic flaps, or percent capillary density ($n = 12$). Bars: (A–D) 500 µm; (I–L) 100 µm. *, $P < 0.05$; **, $P < 0.01$ (compared with control).

Published May 2, 2011

(Phng et al., 2009), and that *Flk-1*$^{-/-}$ embryonic stem cells can differentiate into endothelial cells (Schuh et al., 1999), vascular defects in *Flk-1*$^{Po\text{-}CKO}$ mice are likely caused by impairment in survival and expansion of PVP-derived stalk cells rather than endothelial differentiation of PVPs.

In chick embryos, the dorsal aorta originates from not only the splanchnic mesoderm, but also the somitic mesoderm, which contains tissue-resident mesodermal cells that are distributed before vascular growth (Sato et al., 2008). PVP recruitment in the postnatal retina is similar to the model proposed in this study. Regarding the origin of PVPs, our data and previous studies (Etchevers et al., 2001; Gage et al., 2005) indicate that they are likely derived from the mesoderm but not neural crest. Recently, a differentiation system of human embryonic stem cells (hESCs) identified a common endothelial and mesenchymal cell precursor within a mesodermal subset, called "mesenchymoangioblast" (Vodyanik et al., 2010). Interestingly, this cell population has a potential to differentiate into endothelial cells, as well as mesenchymal stem cells with chondro-, osteo-, and adipogenic differentiation potentials. Po-Cre$^+$ cells in the bone marrow have the potential to give rise to mesenchymal stem cells in an in vitro culture (Morikawa et al., 2009). Our identified PVPs may represent a cell population similar to "mesenchymoangioblast" in the hESC differentiation system (Vodyanik et al., 2010). Interestingly, glioblastoma stemlike cells differentiate into endothelial cells in the tumor vasculature, suggesting plasticity of neural and endothelial lineages, especially during aggressive vascular expansion (Wang et al., 2010; Ricci-Vitiani et al., 2010).

In terms of postnatal vasculogenesis by bone marrow–derived cells, the highly variable extent of the contribution of EPCs may reflect differences in genetic background or the nature of the angiogenic stimulus (Asahara et al., 1997; Gao et al., 2008; Purhonen et al., 2008). Previously, we found there are no Po$^+$ cells in circulation, at least after birth (Nagoshi et al., 2008), suggesting that PVPs are not a kind of so-called EPC, but tissue-resident endothelial precursor cells.

It still remains unclear whether Po is simply a marker of PVPs or also plays a role in the genesis or differentiation of PVPs. *Po*$^{-/-}$ mice develop normally, at least until birth (Giese et al., 1992), and do not show apparent vascular defects in tissue sections from various adult organs (unpublished data). However, *Po*$^{-/-}$ mice are smaller in size than wild-type or heterozygous littermates several weeks after birth, suggesting that some vascular defects may well exist. If we assume that PVPs are defective in *Po*$^{-/-}$ mice, the fact that no major vascular defects occur in *Po*$^{-/-}$ mice is consistent with our conclusion that postnatally growing vessels are primarily formed through angiogenesis from preexisting vessels, and that a minor population of the arterial endothelia is derived from Po$^+$ tissue-resident precursor cells.

In summary, we identified postnatal vascular precursors marked by Po, which exhibit a CD45$^-$CD31$^-$VEcad$^-$c-kit$^+$CXCR4$^+$ surface phenotype. PVPs are recruited into vasculature during physiological development and more actively into expanding capillaries during hypervascular conditions, such as tumor angiogenesis. Future studies may address whether PVP-targeted therapy is a promising strategy for treatment of human neovascular such as cancer.

MATERIALS AND METHODS

Mice. Animal care was performed in accordance with the Guidelines of Keio University for Animal and Recombinant DNA experiments. Transgenic mice expressing Cre recombinase under the control of the Po promoter (*Po-Cre*), the Wnt1 promoter/enhancer (*Wnt1-Cre*), and the Ht-PA promoter (*Ht-PA-Cre*; Pietri et al., 2003) were mated with *Flox-CAT-EGFP* mice (Kawamoto et al., 2000) to obtain *Po-Cre*$^+$*Flox-CAT-EGFP*, *Wnt1-Cre*$^+$*Flox-CAT-EGFP*, and *Ht-PA-Cre*$^+$*Flox-CAT-EGFP* double-transgenic mice. To obtain Po-conditional knockout mice for Flk-1, we initially generated *Po-Cre*$^+$*Flk-1*$^{+/lacZ}$ double-transgenic mice by mating *Po-Cre* mice with *Flk-1*$^{+/lacZ}$ mice (Shalaby et al., 1995). The *Po-Cre*$^+$*Flk-1*$^{+/lacZ}$ mice were then mated with *Flk-1*$^{Flox/Flox}$ mice (Albuquerque et al., 2009). As littermate controls for the conditional knockout mice (*Po-Cre*$^+$*Flk-1*$^{Flox/lacZ}$), we used *Po-Cre*$^-$*Flk-1*$^{Flox/lacZ}$ mice throughout this study.

Preparation of whole-mount samples. Enucleated eyes or other tissues were fixed for 20 min in 4% PFA in PBS, and then dissected. Retinal cups or other tissues were post-fixed and stored in methanol at −20°C.

Whole-mount immunostaining and ISH. IHC of whole-mount samples was performed as previously described (Kubota et al., 2008). For whole-mount ISH, retinas were digested with proteinase K and hybridized with DIG-labeled antisense RNA probes. When ISH was combined with IHC, IHC was performed after ISH procedures were completed as previously described (Fruttiger, 2002). For the BrdU incorporation assay, 100 µg per gram of body weight of BrdU (BD) dissolved in sterile PBS was injected intraperitoneally 2 h before sacrifice. Isolated retinas were stained using a BrdU IHC system (EMD).

Subcutaneous injection of pharmacological reagents. 100 mg/kg DAPT (EMD) dissolved in DMSO was administered subcutaneously (injection volume 10 µl/g body weight). Control mice were injected with vehicle only. Jag1 peptide (CDDYYYGFGCNKFCRPR) or a scrambled peptide (RCGPDCFDNYGRYKYCF; Hellström et al., 2007) was synthesized by Sigma-Aldrich, dissolved at 10 mg/ml in DMSO, and injected (25 µl/injection) subcutaneously. Hamster Dll4-neutralizing antibodies dissolved in sterile PBS at 2.5 mg/ml were injected subcutaneously (25 µl/injection). Control mice were injected with the same amount of nonspecific hamster IgG. TN14003 was dissolved in PBS (0.5 mg/ml) and administered subcutaneously (injection volume 20 µl/g body weight per day).

Antibodies. The primary monoclonal antibodies used were as follows: hamster anti-CD31 (2H8; Millipore), rat anti-CD31 (MEC13.3; BD), PDGFRα (APA5; eBioscience), α-smooth muscle actin (1A4; FITC or Cy3-conjugated; Sigma-Aldrich), GFAP (G-A-5; Cy3-conjugated; Sigma-Aldrich), neurofilament (2H3; Developmental Studies Hybridoma Bank), Pax-6 (Developmental Studies Hybridoma Bank), VE-cadherin (11D4.1; BD), Mac-1 (M1/70; BD), CD45 (BD), F4/80 (CI:A3-1; Serotec), PDGFRβ (APB5; eBioscience), desmin (DAKO), and Dll4 (provided by Hideo Yagita, Juntendo University, Chiba, Japan). The primary polyclonal antibodies used were as follows: anti-GFP (Alexa Fluor 488 conjugated; Invitrogen), Pax-2 (Covance), Flk-1 (Sigma-Aldrich), PDGFRβ (Santa Cruz Biotechnology, Inc.), CD39 (Santa Cruz Biotechnology, Inc.), EphrinB2 (Santa Cruz Biotechnology, Inc.), c-kit (R&D Systems), CXCR4 (eBioscience), Collagen IV (Cosmo Bio), cleaved Notch1 (Cell Signaling Technology), Sox10 (R&D Systems), p75 (EMD), and MBP (Aves Laboratories). Secondary antibodies used were as follows: Alexa 488 fluorescence–conjugated IgGs (Invitrogen) or Cy3/Cy5-conjugated IgGs (Jackson ImmunoResearch Laboratories). For nuclear staining, specimens were treated with TOTO3 (Invitrogen) or DAPI (Invitrogen). In some experiments, blood vessels and monocyte-lineage cells were simultaneously

Published May 2, 2011

visualized using biotinylated isolectin B4 (Sigma-Aldrich), followed by fluorescent streptavidin conjugates (Invitrogen), and vascular precursors were visualized by NeuroTrace Fluorescent Nissl Stains (Invitrogen). For visualization of blood flow, FITC-conjugated Dextran (Sigma-Aldrich) was injected into the left cardiac ventricle and allowed to circulate for 2 min. For FACS analysis, fluorophore- or biotin- conjugated primary antibodies against CD31 (MEC13.3), CXCR4 (BD), c-Kit (2B8; BD), VE-cadherin (BV13; eBioscience), Tie2 (TEK4; eBioscience), PDGFRβ (Santa Cruz Biotechnology, Inc.), Flk-1 (Avas12α1; BD), FGFR1 (QED Bioscience Inc.), CD133 (13A4; eBioscience), SSEA1 (MC-480; eBioscience), PDGFRα (APA5; eBioscience), or CD45 (30F11; BD) were used. Biotin-conjugated antibodies were visualized by incubation with fluorophore-conjugated streptavidin (BD).

Flow cytometric analysis of retinal cells. Retinas of *Po-Cre*$^{+}$*Flox-CAT-EGFP* were incubated for 30 min at 37°C in DMEM containing 1% collagenase D (from *Clostridium histolyticum*) before cells were dissociated by gentle trituration. Dissociated single cells were preincubated with Fc block (BD) to avoid nonspecific binding of antibodies, and then incubated with intended antibodies. Stained samples were analyzed by SORP FACSAria (BD) with FlowJo software (Tree Star) or CellQuest software (BD). Debris and dead cells were excluded by forward and side scatter and a negative gate for propidium iodide staining. Percentages of cell doublets/aggregates were checked by FSC-A versus FSC-W, and SSC-A versus SSC-W plots. In all FACS studies, we routinely included unstained control samples and compensation tubes for FITC, PE, APC, and APC-Cy7. Using these negative and positive control tubes, we set fluorescence voltages and the compensation matrix according to the instructions of the manufacturer. We applied these setting parameters to all the samples that were analyzed.

Quantitative RT-PCR analysis. Total RNA was prepared from FACS-sorted cells or retinal tissues, and reverse transcription was performed using Superscript II (Invitrogen). Quantitative PCR assays were performed on an ABI 7500 Fast Real-Time PCR System using TaqMan Fast Universal PCR master mixture (Applied Biosystems) and TaqMan Gene Expression Assay Mix of *mpz* (Mm00485139_m1), cxcl12 (Mm00445552_m1), or *flk-1* (Mm00440099_m1). A mouse β-*actin* (Mm00607939_s1) assay mix served as an endogenous control. Data were analyzed by 7500 Fast System SDS Software 1.3.1. Each experiment was performed with four replicates from each sample, and the results were averaged.

Cell culture. GFP^{+}CD31^{-}PDGFRβ^{-} cells were isolated from the retinas of *Po-Cre*$^{+}$*Flox-CAT-EGFP* mice by FACS as described above. Cells were washed and resuspended in EGM-II (Cambrex) containing 5% FBS, and then plated on Fibronectin-coated culture slides (BD) at a density of 2×10^4 cells/cm^2. After 4 d of culture, cells were fixed with 4% paraformaldehyde in PBS for 30 min and subjected to IHC.

Intraocular transplantation. Intraocular transplantation of FACS-sorted cells was performed using 33-gauge needles, as described previously (Kubota et al., 2008). In one eye of each wild-type animal at P1, ∼2,000 cells suspended in 0.2 µl of DMEM containing 2% FBS were gently injected just between the iris and retina under a microscope. Recipient mice were sacrificed at P6. In some experiments, PVPs isolated from P3 retinas were preincubated with the CXCR4 antagonist, TN14003 (4 µg/ml; Tamamura et al., 2001) or vehicle for 60 min in DMEM containing 2% FBS, and transplanted into the retinas of P3 mice. Recipient mice were sacrificed at P5.

Chemotaxis assay. The chemotaxis assay was performed using Transwell membrane filters (8.0-µm pore; Corning). Both the upper and lower surfaces of the membranes were coated with 0.1% gelatin. 600 µl of EBM-2 containing 0.2% FBS, with or without indicated concentrations of CXCL12 (R&D Systems), was added to the lower wells of 24-well plates. PVPs (GFP^{+}CD31^{-}PDGFRβ^{-}) were isolated from the retinas of *Po-Cre*$^{+}$*Flox-CAT-EGFP* mice by FACS as described in the Flow cytometric analysis of retinal cells section. Cells were resuspended in EBM-2 containing 0.2% FBS, added to the upper wells (2×10^4 cells/well), and incubated for 4 h. Cells were then fixed by 100% methanol, washed, and stained with hematoxylin solution. In some experiments, PVPs were preincubated with the CXCR4 antagonist, TN14003 (4 µg/ml), or control medium for 30 min in EBM-2 containing 0.2% FBS. The number of cells attached to the lower surface of the membranes was counted microscopically. Cells were counted in 10 randomly chosen high-power fields on the membrane, and an average number was obtained. Experiments were repeated 4 times.

Tumor transplantation model. Sarcoma 180 (S-180) murine transplantable tumor cells (provided by T. Shindo, Shinshu University Graduate School of Medicine, Matsumoto, Nagano, Japan) that had been cultured in the abdomen were isolated from the ascites. After removal of red blood cells, tumor cells were transplanted by subcutaneous injection into the bilateral axillae of 15-wk-old male mice at a dose of 2×10^6 cells in 0.2 ml per mouse. Tumors were removed for analysis 10 d after transplantation.

Ischemic flap model. Dorsal flaps (1 × 5 cm) were introduced onto the backs of 15-wk-old male mice in a modification of the previous study (Ceradini et al., 2004). The flaps were raised with the base at the tail end, including intimately attached panniculus carnosus. The flaps were then sutured back to the donor bed using 4–0 Nylon. Ischemic tissues in the distal end of the flaps were harvested for analysis 7 d after flap elevation. Necrotic areas were quantified using ImageJ Software (National Institutes of Health).

Confocal microscopy. Fluorescent images were obtained using a confocal laser scanning microscope (FV1000; Olympus). Quantification of cells or substances of interest was done on eight 200 × 200 µm fields of view per sample in scanned images, and numbers obtained from each of the eight fields were averaged. Scion image software (Scion Corporation) was used for quantification of fluorescence intensity or capillary density in confocal images.

Statistical analysis. All results are expressed as mean ± SD. The comparison between the averaged variables of two groups was evaluated using the two-tailed Student's *t* test. $P < 0.05$ was considered statistically significant.

Online supplemental material. Fig. S1 shows the IHC data showing that Po-Cre^{+} spindle-shaped cells are negative for pericytic, neuronal, and hematopoietic markers. Fig. S2 shows the IHC data showing that Po-Cre does not mark embryonic endothelial cells. Fig. S3 shows the data showing that Dll4 neutralization enhance the recruitment of PVPs. Fig. S4 shows the IHC data showing that Flk-1 expression in *Flk-1*$^{Po\text{-}CKO}$ mice show reduction in endothelial cells but not in Muller cells and photoreceptors. Fig. S5 shows the IHC data showing that Flk-1 is expressed in endothelial cells, but not neural crest cells, neurons, Schwann cells, or pericytes/vSMCs. Fig. S6 shows the IHC data showing that *Flk-1*$^{Po\text{-}CKO}$ mice show decreased endothelial proliferation, increased endothelial apoptosis, and increased vessel regression. Online supplemental material is available at http://www.jem.org/cgi/content/full/jem.20102187/DC1.

We thank Hideo Yagita for providing us with the hamster Dll4-neutralizing antibodies. We thank Takayuki Shindo for providing us with the Sarcoma-180 cells. We thank Takashi Yamamura (National Center of Neurology and Psychiatry, Japan) for his helpful discussion.

This work was supported by Grants-in-Aid for Specially Promoted Research from the Ministry of Education, Culture, Sports, Science and Technology of Japan, by a grant from the Mitsubishi Pharma Research Foundation, and by the Keio Kanrinmaru Project.

The authors have no competing financial interests associated with this publication.

Submitted: 14 October 2010
Accepted: 22 March 2011

REFERENCES

Albuquerque, R.J., T. Hayashi, W.G. Cho, M.E. Kleinman, S. Dridi, A. Takeda, J.Z. Baffi, K. Yamada, H. Kaneko, M.G. Green, et al. 2009. Alternatively spliced vascular endothelial growth factor receptor-2 is an essential endogenous inhibitor of lymphatic vessel growth. *Nat. Med.* 15:1023–1030. doi:10.1038/nm.2018

Asahara, T., T. Murohara, A. Sullivan, M. Silver, R. van der Zee, T. Li, B. Witzenbichler, G. Schatteman, and J.M. Isner. 1997. Isolation of putative progenitor endothelial cells for angiogenesis. *Science*. 275:964–967. doi:10.1126/science.275.5302.964

Ashton, N. 1970. Retinal angiogenesis in the human embryo. *Br. Med. Bull.* 26:103–106.

Beltrami, A.P., L. Barlucchi, D. Torella, M. Baker, F. Limana, S. Chimenti, H. Kasahara, M. Rota, E. Musso, K. Urbanek, et al. 2003. Adult cardiac stem cells are multipotent and support myocardial regeneration. *Cell.* 114:763–776. doi:10.1016/S0092-8674(03)00687-1

Carmeliet, P. 2003. Angiogenesis in health and disease. *Nat. Med.* 9:653–660. doi:10.1038/nm0603-653

Ceradini, D.J., A.R. Kulkarni, M.J. Callaghan, O.M. Tepper, N. Bastidas, M.E. Kleinman, J.M. Capla, R.D. Galiano, J.P. Levine, and G.C. Gurtner. 2004. Progenitor cell trafficking is regulated by hypoxic gradients through HIF-1 induction of SDF-1. *Nat. Med.* 10:858–864. doi:10.1038/nm1075

Danielian, P.S., D. Muccino, D.H. Rowitch, S.K. Michael, and A.P. McMahon. 1998. Modification of gene activity in mouse embryos in utero by a tamoxifen-inducible form of Cre recombinase. *Curr. Biol.* 8:1323–1326. doi:10.1016/S0960-9822(07)00562-3

Ema, M., T. Yokomizo, A. Wakamatsu, T. Terunuma, M. Yamamoto, and S. Takahashi. 2006. Primitive erythropoiesis from mesodermal precursors expressing VE-cadherin, PECAM-1, Tie2, endoglin, and CD34 in the mouse embryo. *Blood.* 108:4018–4024. doi:10.1182/blood-2006-03-012872

Etchevers, H.C., C. Vincent, N.M. Le Douarin, and G.F. Couly. 2001. The cephalic neural crest provides pericytes and smooth muscle cells to all blood vessels of the face and forebrain. *Development.* 128:1059–1068.

Fruttiger, M. 2002. Development of the mouse retinal vasculature: angiogenesis versus vasculogenesis. *Invest. Ophthalmol. Vis. Sci.* 43:522–527.

Gage, P.J., W. Rhoades, S.K. Prucka, and T. Hjalt. 2005. Fate maps of neural crest and mesoderm in the mammalian eye. *Invest. Ophthalmol. Vis. Sci.* 46:4200–4208. doi:10.1167/iovs.05-0691

Gao, D., D.J. Nolan, A.S. Mellick, K. Bambino, K. McDonnell, and V. Mittal. 2008. Endothelial progenitor cells control the angiogenic switch in mouse lung metastasis. *Science.* 319:195–198. doi:10.1126/science.1150224

Gariano, R.F., and T.W. Gardner. 2005. Retinal angiogenesis in development and disease. *Nature.* 438:960–966. doi:10.1038/nature04482

Gerhardt, H., M. Golding, M. Fruttiger, C. Ruhrberg, A. Lundkvist, A. Abramsson, M. Jeltsch, C. Mitchell, K. Alitalo, D. Shima, and C. Betsholtz. 2003. VEGF guides angiogenic sprouting utilizing endothelial tip cell filopodia. *J. Cell Biol.* 161:1163–1177. doi:10.1083/jcb.200302047

Giese, K.P., R. Martini, G. Lemke, P. Soriano, and M. Schachner. 1992. Mouse P0 gene disruption leads to hypomyelination, abnormal expression of recognition molecules, and degeneration of myelin and axons. *Cell.* 71:565–576. doi:10.1016/0092-8674(92)90591-Y

Grenier, G., A. Scimè, F. Le Grand, A. Asakura, C. Perez-Iratxeta, M.A. Andrade-Navarro, P.A. Labosky, and M.A. Rudnicki. 2007. Resident endothelial precursors in muscle, adipose, and dermis contribute to postnatal vasculogenesis. *Stem Cells.* 25:3101–3110. doi:10.1634/stemcells.2006-0795

Guo, Y., B. Graham-Evans, and H.E. Broxmeyer. 2006. Murine embryonic stem cells secrete cytokines/growth modulators that enhance cell survival/anti-apoptosis and stimulate colony formation of murine hematopoietic progenitor cells. *Stem Cells.* 24:850–856. doi:10.1634/stemcells.2005-0457

Hellström, M., L.K. Phng, J.J. Hofmann, E. Wallgard, L. Coultas, P. Lindblom, J. Alva, A.K. Nilsson, L. Karlsson, N. Gaiano, et al. 2007. Dll4 signalling through Notch1 regulates formation of tip cells during angiogenesis. *Nature.* 445:776–780. doi:10.1038/nature05571

Henking, P., and L.F. De Oliveira. 1967. Development of retinal vessels in the rat. *Invest. Ophthalmol.* 6:520–530.

Jakobsson, L., C.A. Franco, K. Bentley, R.T. Collins, B. Ponsioen, I.M. Aspalter, I. Rosewell, M. Busse, G. Thurston, A. Medvinsky, et al. 2010. Endothelial cells dynamically compete for the tip cell position during angiogenic sprouting. *Nat. Cell Biol.* 12:943–953. doi:10.1038/ncb2103

Jiang, Y., B. Vaessen, T. Lenvik, M. Blackstad, M. Reyes, and C.M. Verfaillie. 2002. Multipotent progenitor cells can be isolated from postnatal murine bone marrow, muscle, and brain. *Exp. Hematol.* 30:896–904. doi:10.1016/S0301-472X(02)00869-X

Jin, D.K., K. Shido, H.G. Kopp, I. Petit, S.V. Shmelkov, L.M. Young, A.T. Hooper, H. Amano, S.T. Avecilla, B. Heissig, et al. 2006. Cytokine-mediated deployment of SDF-1 induces revascularization through recruitment of CXCR4+ hemangiocytes. *Nat. Med.* 12:557–567. doi:10.1038/nm1400

Kawamoto, S., H. Niwa, F. Tashiro, S. Sano, G. Kondoh, J. Takeda, K. Tabayashi, and J. Miyazaki. 2000. A novel reporter mouse strain that expresses enhanced green fluorescent protein upon Cre-mediated recombination. *FEBS Lett.* 470:263–268. doi:10.1016/S0014-5793(00)01338-7

Kubota, Y., M. Hirashima, K. Kishi, C.L. Stewart, and T. Suda. 2008. Leukemia inhibitory factor regulates microvessel density by modulating oxygen-dependent VEGF expression in mice. *J. Clin. Invest.* 118:2393–2403.

Lawson, N.D., A.M. Vogel, and B.M. Weinstein. 2002. sonic hedgehog and vascular endothelial growth factor act upstream of the Notch pathway during arterial endothelial differentiation. *Dev. Cell.* 3:127–136. doi:10.1016/S1534-5807(02)00198-3

Lemke, G., and R. Axel. 1985. Isolation and sequence of a cDNA encoding the major structural protein of peripheral myelin. *Cell.* 40:501–508. doi:10.1016/0092-8674(85)90198-9

McLeod, D.S., T. Hasegawa, T. Prow, C. Merges, and G. Lutty. 2006. The initial fetal human retinal vasculature develops by vasculogenesis. *Dev. Dyn.* 235:3336–3347. doi:10.1002/dvdy.20988

Millauer, B., S. Wizigmann-Voos, H. Schnürch, R. Martinez, N.P. Møller, W. Risau, and A. Ullrich. 1993. High affinity VEGF binding and developmental expression suggest Flk-1 as a major regulator of vasculogenesis and angiogenesis. *Cell.* 72:835–846. doi:10.1016/0092-8674(93)90573-9

Morikawa, S., Y. Mabuchi, K. Niibe, S. Suzuki, N. Nagoshi, T. Sunabori, S. Shimmura, Y. Nagai, T. Nakagawa, H. Okano, and Y. Matsuzaki. 2009. Development of mesenchymal stem cells partially originate from the neural crest. *Biochem. Biophys. Res. Commun.* 379:1114–1119. doi:10.1016/j.bbrc.2009.01.031

Nagoshi, N., S. Shibata, Y. Kubota, M. Nakamura, Y. Nagai, E. Satoh, S. Morikawa, Y. Okada, Y. Mabuchi, H. Katoh, et al. 2008. Ontogeny and multipotency of neural crest-derived stem cells in mouse bone marrow, dorsal root ganglia, and whisker pad. *Cell Stem Cell.* 2:392–403. doi:10.1016/j.stem.2008.03.005

Noguera-Troise, I., C. Daly, N.J. Papadopoulos, S. Coetzee, P. Boland, N.W. Gale, H.C. Lin, G.D. Yancopoulos, and G. Thurston. 2006. Blockade of Dll4 inhibits tumour growth by promoting non-productive angiogenesis. *Nature.* 444:1032–1037. doi:10.1038/nature05355

Phng, L.K., M. Potente, J.D. Leslie, J. Babbage, D. Nyqvist, I. Lobov, J.K. Ondr, S. Rao, R.A. Lang, G. Thurston, and H. Gerhardt. 2009. Nrarp coordinates endothelial Notch and Wnt signaling to control vessel density in angiogenesis. *Dev. Cell.* 16:70–82. doi:10.1016/j.devcel.2008.12.009

Pietri, T., O. Eder, M. Blanche, J.P. Thiery, and S. Dufour. 2003. The human tissue plasminogen activator-Cre mouse: a new tool for targeting specifically neural crest cells and their derivatives in vivo. *Dev. Biol.* 259:176–187. doi:10.1016/S0012-1606(03)00175-1

Planat-Benard, V., J.S. Silvestre, B. Cousin, M. André, M. Nibbelink, R. Tamarat, M. Clergue, C. Manneville, C. Saillan-Barreau, M. Duriez, et al. 2004. Plasticity of human adipose lineage cells toward endothelial cells: physiological and therapeutic perspectives. *Circulation.* 109:656–663. doi:10.1161/01.CIR.0000114522.38265.61

Purhonen, S., J. Palm, D. Rossi, N. Kaskenpää, I. Rajantie, S. Ylä-Herttuala, K. Alitalo, I.L. Weissman, and P. Salven. 2008. Bone marrow-derived circulating endothelial precursors do not contribute to vascular endothelium and are not needed for tumor growth. *Proc. Natl. Acad. Sci. USA.* 105:6620–6625. doi:10.1073/pnas.0710516105

Ratajczak, M.Z., E.K. Zuba-Surma, B. Machalinski, J. Ratajczak, and M. Kucia. 2008. Very small embryonic-like (VSEL) stem cells: purification from adult organs, characterization, and biological significance. *Stem Cell Rev.* 4:89–99. doi:10.1007/s12015-008-9018-0

Ricci-Vitiani, L., R. Pallini, M. Biffoni, M. Todaro, G. Invernici, T. Cenci, G. Maira, E.A. Parati, G. Stassi, L.M. Larocca, and R. De Maria. 2010. Tumour vascularization via endothelial differentiation of glioblastoma stem-like cells. *Nature*. 468:824–828. doi:10.1038/nature09557

Ridgway, J., G. Zhang, Y. Wu, S. Stawicki, W.C. Liang, Y. Chanthery, J. Kowalski, R.J. Watts, C. Callahan, I. Kasman, et al. 2006. Inhibition of Dll4 signalling inhibits tumour growth by deregulating angiogenesis. *Nature*. 444:1083–1087. doi:10.1038/nature05313

Risau, W. 1997. Mechanisms of angiogenesis. *Nature*. 386:671–674. doi:10.1038/386671a0

Sato, Y., T. Watanabe, D. Saito, T. Takahashi, S. Yoshida, J. Kohyama, E. Ohata, H. Okano, and Y. Takahashi. 2008. Notch mediates the segmental specification of angioblasts in somites and their directed migration toward the dorsal aorta in avian embryos. *Dev. Cell*. 14:890–901. doi:10.1016/j.devcel.2008.03.024

Schuh, A.C., P. Faloon, Q.L. Hu, M. Bhimani, and K. Choi. 1999. In vitro hematopoietic and endothelial potential of flk-1(−/−) embryonic stem cells and embryos. *Proc. Natl. Acad. Sci. USA*. 96:2159–2164. doi:10.1073/pnas.96.5.2159

Shalaby, F., J. Rossant, T.P. Yamaguchi, M. Gertsenstein, X.F. Wu, M.L. Breitman, and A.C. Schuh. 1995. Failure of blood-island formation and vasculogenesis in Flk-1-deficient mice. *Nature*. 376:62–66. doi:10.1038/376062a0

Stern, C.D., and S.E. Fraser. 2001. Tracing the lineage of tracing cell lineages. *Nat. Cell Biol.* 3:E216–E218. doi:10.1038/ncb0901-e216

Suchting, S., C. Freitas, F. le Noble, R. Benedito, C. Bréant, A. Duarte, and A. Eichmann. 2007. The Notch ligand Delta-like 4 negatively regulates endothelial tip cell formation and vessel branching. *Proc. Natl. Acad. Sci. USA*. 104:3225–3230. doi:10.1073/pnas.0611177104

Tamamura, H., A. Omagari, K. Hiramatsu, K. Gotoh, T. Kanamoto, Y. Xu, E. Kodama, M. Matsuoka, T. Hattori, N. Yamamoto, et al. 2001. Development of specific CXCR4 inhibitors possessing high selectivity indexes as well as complete stability in serum based on an anti-HIV peptide T140. *Bioorg. Med. Chem. Lett.* 11:1897–1902. doi:10.1016/S0960-894X(01)00323-7

Tammela, T., G. Zarkada, E. Wallgard, A. Murtomäki, S. Suchting, M. Wirzenius, M. Waltari, M. Hellström, T. Schomber, R. Peltonen, et al. 2008. Blocking VEGFR-3 suppresses angiogenic sprouting and vascular network formation. *Nature*. 454:656–660. doi:10.1038/nature07083

Vodyanik, M.A., J. Yu, X. Zhang, S. Tian, R. Stewart, J.A. Thomson, and I.I. Slukvin. 2010. A mesoderm-derived precursor for mesenchymal stem and endothelial cells. *Cell Stem Cell*. 7:718–729. doi:10.1016/j.stem.2010.11.011

Wang, R., K. Chadalavada, J. Wilshire, U. Kowalik, K.E. Hovinga, A. Geber, B. Fligelman, M. Leversha, C. Brennan, and V. Tabar. 2010. Glioblastoma stem-like cells give rise to tumour endothelium. *Nature*. 468:829–833. doi:10.1038/nature09624

Wurmser, A.E., K. Nakashima, R.G. Summers, N. Toni, K.A. D'Amour, D.C. Lie, and F.H. Gage. 2004. Cell fusion-independent differentiation of neural stem cells to the endothelial lineage. *Nature*. 430:350–356. doi:10.1038/nature02604

Yamauchi, Y., K. Abe, A. Mantani, Y. Hitoshi, M. Suzuki, F. Osuzu, S. Kuratani, and K. Yamamura. 1999. A novel transgenic technique that allows specific marking of the neural crest cell lineage in mice. *Dev. Biol.* 212:191–203. doi:10.1006/dbio.1999.9323

SUPPLEMENTAL MATERIAL

Kubota et al., http://www.jem.org/cgi/content/full/jem.20102187/DC1

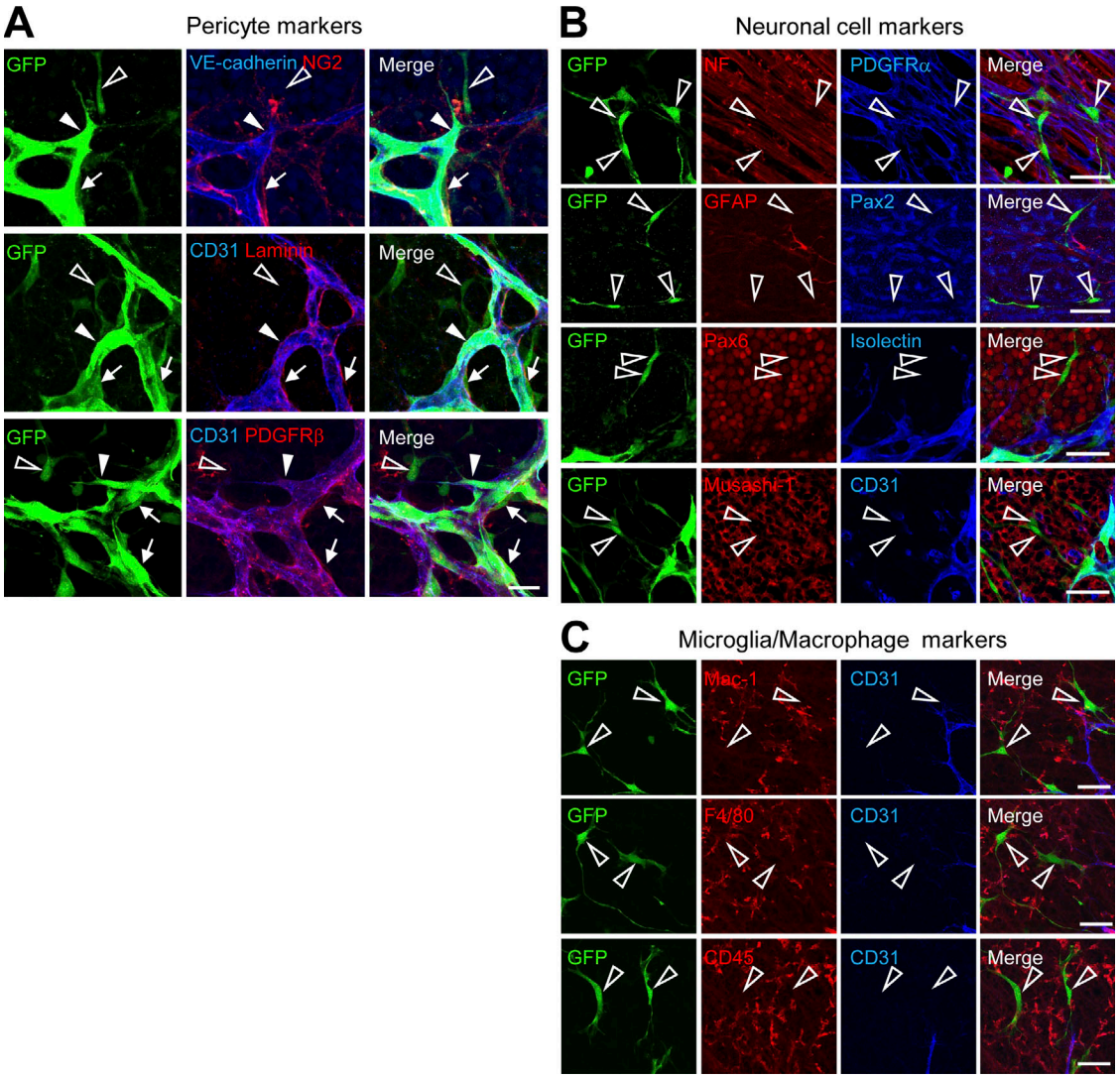

Figure S1. Characterization of Po-Cre$^+$ spindle-shaped cells in the avascular area. IHC of retinas from *Po-Cre$^+$Flox-CAT-EGFP* mice at P4 stained with antibodies of markers for pericytes (A), astrocytes/neurons/retinal progenitors/photoreceptors (B), and microglia/macrophages (C). Representative images from at least three independent experiments. Pericytes (arrows). GFP$^+$ spindle-shaped cells (open arrowheads). GFP$^+$ endothelial cells (closed arrowheads). Bars: (B and C) 50 µm; (A) 20 µm.

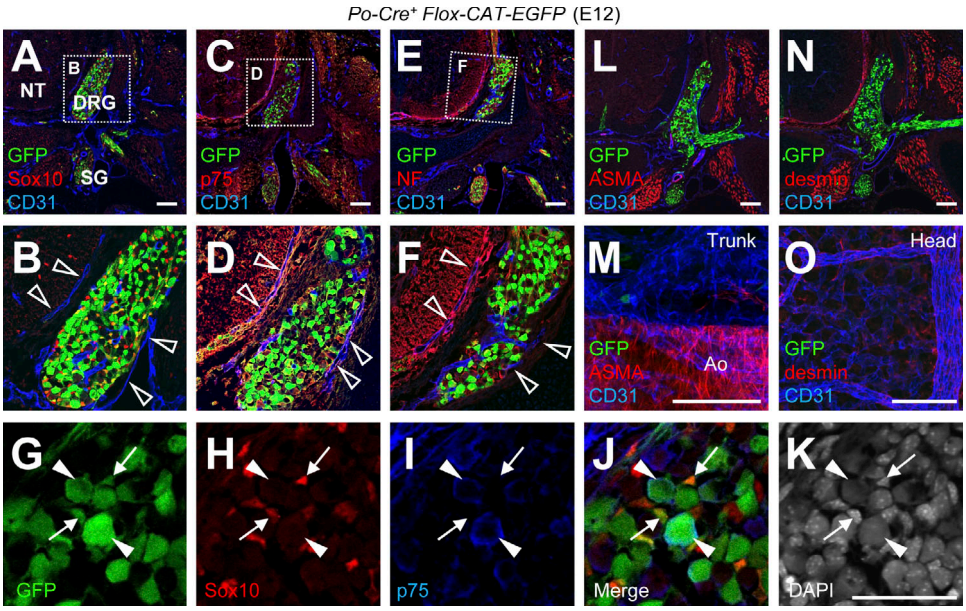

Figure S2. Po-Cre does not mark embryonic endothelial cells. Trunk sections (A–L and N) or whole-mount samples (M and O) of *Po-Cre*$^{+}$*Flox-CAT-EGFP* embryos (E12) immunostained with indicated antibodies. Representative images from at least three independent experiments. Ao, dorsal aorta. DRG, dorsal root ganglia; SG, sympathetic ganglia; NT, neural tube. Open arrowheads, endothelial cells. GFP^{+}sox10^{+} cells (arrows in G-K). GFP^{+}p75^{+} cells (closed arrowheads in G–K). Bars, 50 µm.

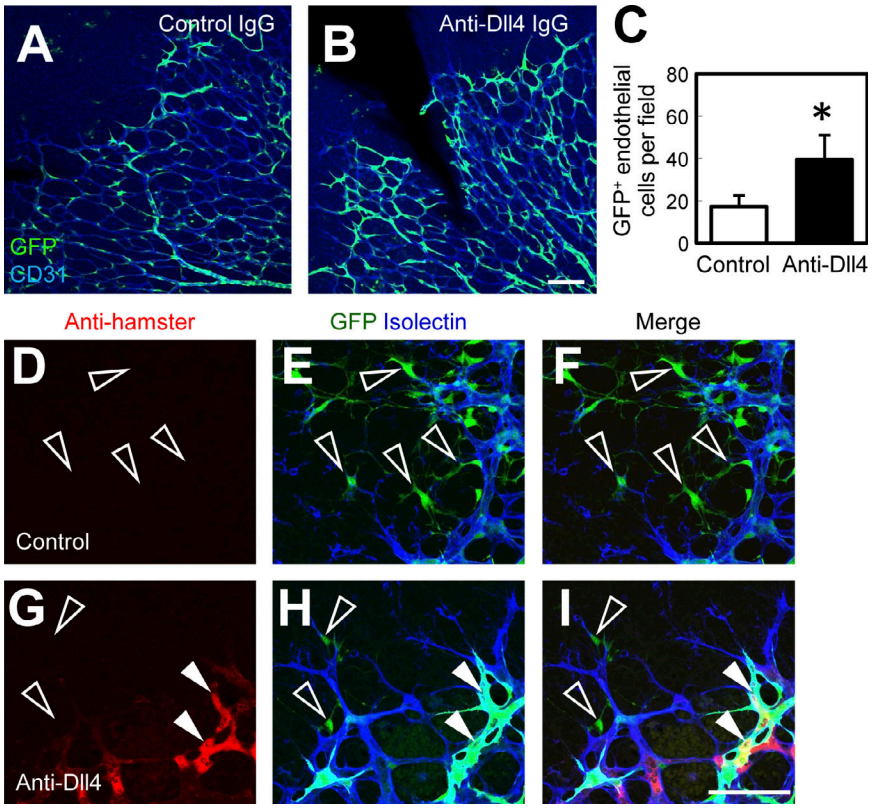

Figure S3. Recruitment of PVPs is enhanced by Dll4 neutralization. (A and B) IHC for GFP (green) and CD31 (blue) in P5 retinas of *Po-Cre*$^{+}$*Flox-CAT-EGFP* mice after pulse treatment from P1 to P5 with hamster IgGs (A) or Dll4 neutralizing antibodies (B). Representative images from eight independent experiments. (C) Quantification of GFP^{+} endothelial cells ($n = 8$). (D–I) Immunostaining with anti-hamster IgG combined with IHC for GFP (green) and CD31 (blue) in retinas of P5 *Po-Cre*$^{+}$*Flox-CAT-EGFP* mice 12 h after treatment with hamster IgGs or Dll4 neutralizing antibodies. Representative images from three independent experiments. Closed arrowheads, GFP^{+} endothelial cells. Open arrowheads, PVPs. Bars, 100 µm. *, $P < 0.05$.

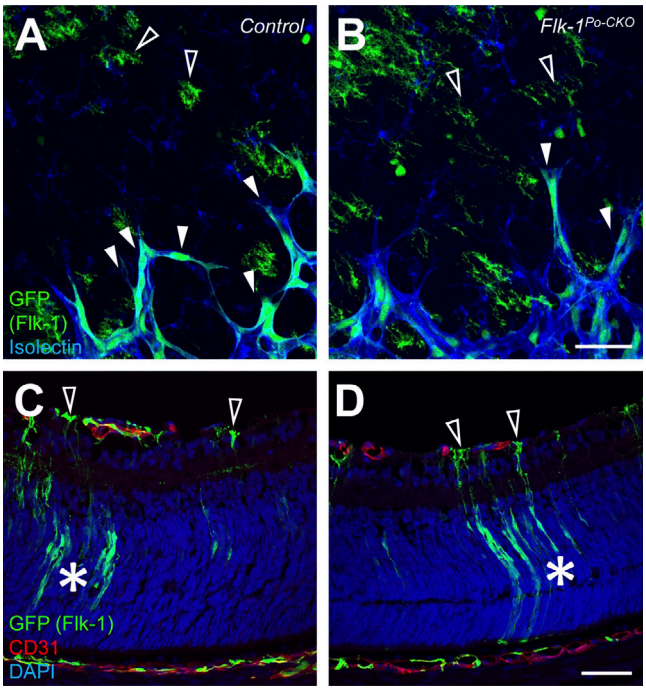

Figure S4. Flk-1 expression in Flk-1$^{Po\text{-}CKO}$ mice shows reduction in endothelial cells, but not in Muller cells and photoreceptors. (A and B) Whole-mount IHC for GFP (green) and Isolectin (blue) in P5 retinas of *Flk-1$^{Flox/EGFP}$* mice (control) or *Po-Cre^{+}Flk-1$^{Flox/EGFP}$* (*Flk-1$^{Po\text{-}CKO}$*) mice. Representative images from three independent experiments. Closed arrowheads, endothelial cells. Open arrowheads, Muller cells. (C and D) Section IHC in P5 retinas of *Flk-1$^{Flox/EGFP}$* mice (control) or *Po-Cre/Flk-1$^{Flox/EGFP}$* (*Flk-1$^{Po\text{-}CKO}$*) mice. Representative images from three independent experiments. Asterisks represent hotoreceptors in the outer nuclear layer. Open arrowheads, Muller cells. Bars, 50 µm.

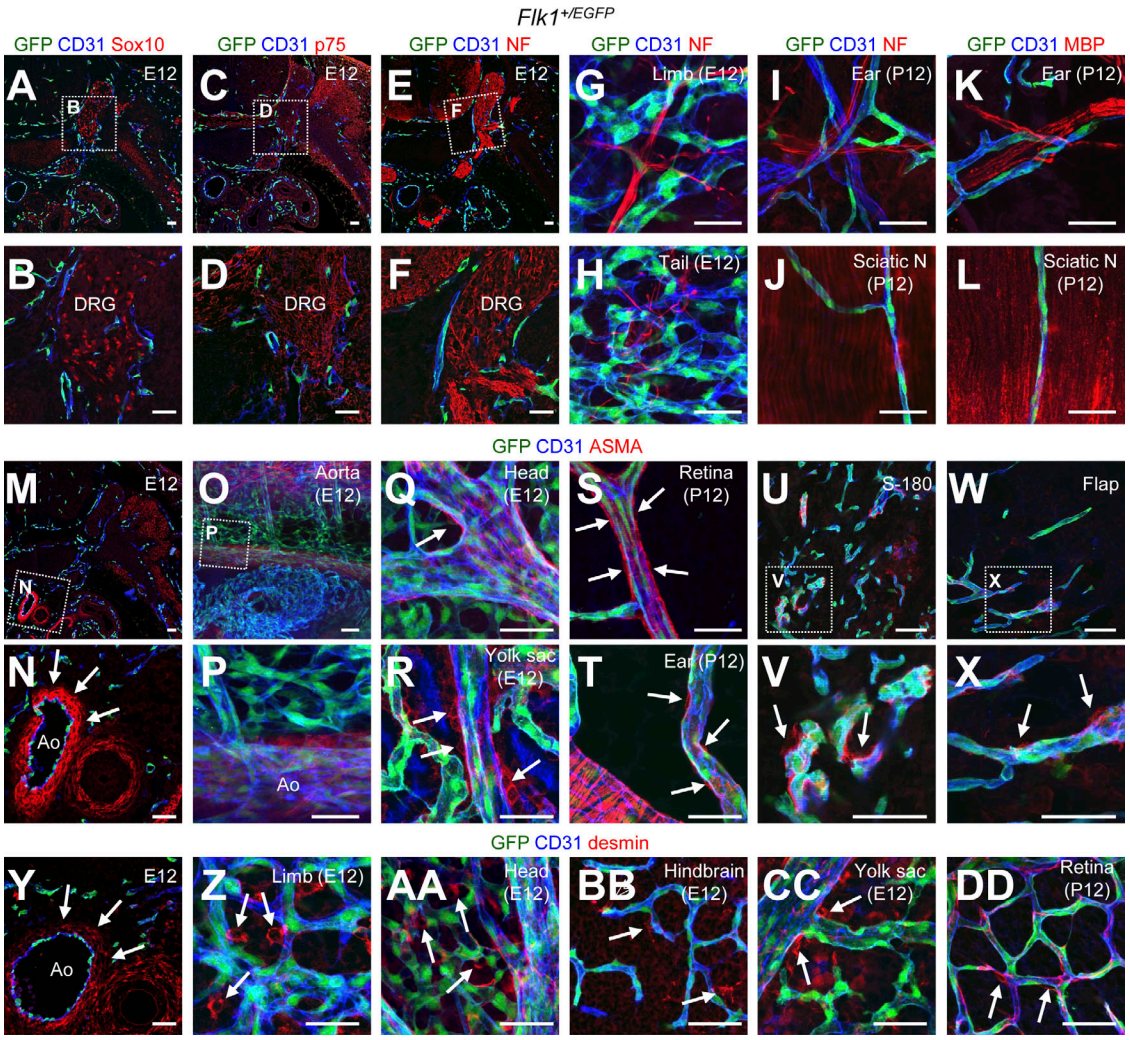

Figure S5. Flk-1 is expressed in endothelial cells, but not neural crest cells, neurons, Schwann cells, or pericytes/vSMCs. IHC with the indicated antibodies in various tissues harvested from *Flk-1*$^{+/EGFP}$ mice at E12, P12, 10 d after S-180 transplantation (3 mo old), or 7 d after ischemic flap elevation (3 mo old). Representative images from at least three independent experiments. Dorsal root ganglia (DRG). Pericytes/vSMCs (arrows). Dorsal Aorta (Ao). Bars, 50 µm.

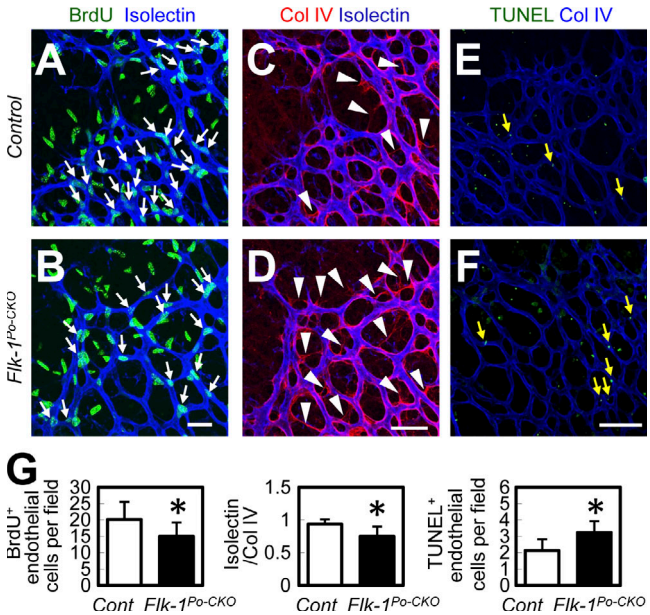

Figure S6. Flk-1$^{Po\text{-}CKO}$ mice show decreased endothelial proliferation, increased endothelial apoptosis, and increased vessel regression. (A–F) IHC with indicated antibodies. Arrows, endothelial proliferation. Arrowheads, empty sleeves. Yellow arrows, apoptosis. Representative images from eight independent experiments. (G) Quantification of BrdU$^+$ endothelial cells, ratio of IsolectinB4$^+$ vessels to collagen IV$^+$ vessels, and TUNEL$^+$ endothelial cells (n = 8, respectively). Bars, 100 µm.